

AGNS AND CLUSTERS IN CHANDRA DEEP FIELDS

P. TOZZI¹ AND THE CDFS TEAM

¹*Osservatorio Astronomico di Trieste, via G.B. Tiepolo 11, I-34131, Trieste, Italy*

Abstract. The Chandra X-ray Satellite already observed several deep fields, including the two 1 Megasec exposures of the Chandra Deep Field South (CDFS) and North. We review here the main findings from the CDFS. The LogN–LogS relations show the resolution of the X-ray background into point sources at the level of 83–99% in the 1–2 keV band and 65–98% in the 2–10 keV band, given the uncertainties in the unresolved value. The so called “spectral paradox” is solved by a hard, faint population of sources constituted mostly by nearby ($z \leq 1$) absorbed (Type II) AGNs with hard-band luminosities $L \simeq 10^{42} - 10^{44}$ erg s⁻¹. When comparing these results to other deep fields in the X-ray band, we find that the AGNs detected in 0.1 deg² of the CDFS are representative of the AGNs population as a whole. However, we also noticed an excess in the hard counts in two Chandra deep fields. If we include this excess and average it among the observed fields, the total contribution of the XRB can grow of about 7%. Finally, we discuss briefly the properties of the Intra Cluster Medium imaged at high z , showing no evolution in clusters properties up to $z \simeq 1$.

1 Introduction

In the 940 ks exposure (hereafter 1Ms) of the Chandra Deep Field South (Giacconi et al. 2001; Tozzi et al. 2001; Rosati et al. 2001, hereafter Paper I, II and III) we reached an on-axis flux limit of $S = 4.5 \times 10^{-16}$ erg s⁻¹ cm⁻² and $S = 5.5 \times 10^{-17}$ erg s⁻¹ cm⁻² in the hard (2–10 keV) and soft (0.5–2 keV) band respectively. This is the deepest X-ray exposure to date together with the 1 Megasec exposure reached in the Hubble Deep Field North by the Penn State University group (see Hornschemeier et al. 2000; 2001; Brandt et al. 2000). These, and other deep fields of few $\times 10^5$ sec, are now public in the Chandra Archive. To these deep looks into the X-ray sky, we can add the 100 ksec observation of the Lockman Hole with XMM (Hasinger et al. 2001).

In these Proceedings we summarize the results from the X-ray data of the CDFS, namely the soft and hard counts, the contribution to the X-ray background (XRB), and some X-ray spectral properties of the sample. We will also compare the results of the CDFS with other deep fields. Finally, we will briefly discuss the properties of the Intra Cluster Medium (ICM) detected in high- z clusters of galaxies. This is just a quick look through the window opened by Chandra and XMM on the high- z , X-ray sky.

2 Results from the Chandra Deep Field South

The Chandra Deep Field South (CDFS) data have been obtained by adding 11 pointings of the Chandra satellite from October 1999 to December 2000. The pointings had different roll angles, enabling a total coverage of 0.1089 deg². The data were reduced with the standard software developed at the CfA (CIAO release V1.5, see <http://asc.harvard.edu/cda>) and the source detection process is described in detail in Papers I and II. The energy fluxes are obtained from the observed net count-rates using a count-rate to flux conversion factors for an average photon index $\Gamma = 1.4$ and a Galactic absorbing column of 8×10^{19} cm⁻². The conversion factors are $(4.6 \pm 0.1) \times 10^{-12}$ erg s⁻¹ cm⁻² per count s⁻¹, and $(2.9 \pm 0.3) \times 10^{-11}$ erg s⁻¹ cm⁻² per count s⁻¹ in the soft and in the hard band respectively. The source count rates are corrected for vignetting and varying exposure time across the field.

In the soft band the differential counts are well fitted by a double power law which is consistent with the Euclidean slope at the bright end and with a slope $\alpha_{diff} \equiv \alpha + 1 = 1.63 \pm 0.13$ (1 sigma

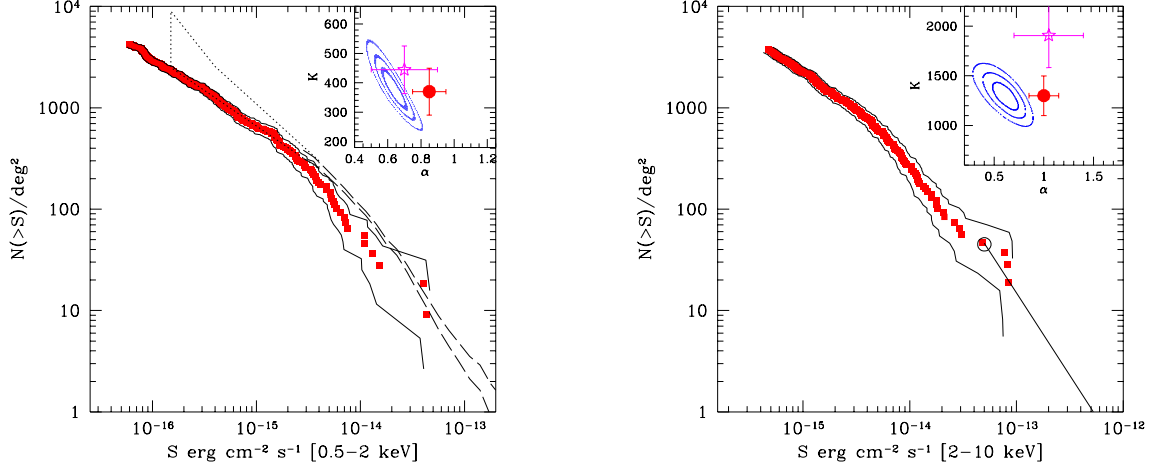


Figure 1: Left: The LogN–LogS in the soft band from the CDFS for an average spectral slope $\Gamma = 1.4$ (filled squares). Dashed lines are the counts from the Lockman Hole (Hasinger et al. 1998), and the dotted contour is the extrapolation from the fluctuation analysis in ROSAT data (Hasinger et al. 1993). The upper and lower solid lines indicate uncertainties due to the sum of the Poisson noise (1 sigma) including the uncertainty in the conversion factor. The insert shows the maximum likelihood contours to the slope and normalization of the faint end of the number counts from the double power law fit (the normalization is defined at $S = 2 \times 10^{-15}$ erg s $^{-1}$ cm $^{-2}$). The contours correspond to 1σ , 2σ and 3σ . The star is the single power law fit from Mushotzky et al. (2000) at $S = 2 \times 10^{-15}$ erg s $^{-1}$ cm $^{-2}$; the error bar is their quoted 68% confidence level. The large dot is the single power law fit from Paper I. Right: The LogN–LogS in the hard band. The open circle at high fluxes is from ASCA and Beppo SAX (Giommi, Perri & Fiore 2000; Ueda et al. 1999) and the solid line is the fit to the counts from ASCA in the range $10^{-12} - 10^{-13}$ erg cm $^{-2}$ s $^{-1}$ (Della Ceca et al. 2000).

error) at the faint end, with a break at $S \simeq 1.5 \times 10^{-14}$ erg s $^{-1}$ cm $^{-2}$ (see Paper III). Thus, below $S \sim 10^{-15}$ erg s $^{-1}$ cm $^{-2}$, the slope of the cumulative number counts is $\alpha \simeq 0.6$ (see Figure 1, left), showing that we are about to saturate the XRB. In the 1–2 keV band we find a resolved contribution of $\simeq 6.25 \times 10^{-13}$ erg s $^{-1}$ cm $^{-2}$ deg $^{-2}$ for fluxes lower than 10^{-15} erg s $^{-1}$ cm $^{-2}$, corresponding to $\simeq 14 - 17\%$ of the unresolved flux measured by ROSAT (which is 4.4×10^{-12} erg s $^{-1}$ cm $^{-2}$, see Hasinger et al. 1998). If this value is summed to the contribution at higher fluxes, we estimate a total contribution of $\simeq 3.65 \times 10^{-12}$ erg s $^{-1}$ cm $^{-2}$ deg $^{-2}$ for fluxes larger than 3×10^{-17} erg s $^{-1}$ cm $^{-2}$ (which is our flux limit in the 1–2 keV band), corresponding to 83% of the unresolved value.

In the hard counts too, we find evidence for progressive flattening: the differential counts are well fitted by a power law which is consistent with the Euclidean slope at the bright end and with a slope $\alpha_{diff} = 1.58 \pm 0.12$ (1 sigma) at the faint end, with a break at $S \simeq 8.4 \times 10^{-15}$ erg s $^{-1}$ cm $^{-2}$ (see Figure 1, right). The integrated contribution of all the sources within the flux range 10^{-13} erg s $^{-1}$ cm $^{-2}$ to 4.5×10^{-16} erg s $^{-1}$ cm $^{-2}$ in the 2–10 keV band is $(1.31 \pm 0.20) \times 10^{-11}$ erg s $^{-1}$ cm $^{-2}$ deg $^{-2}$ for $\Gamma = 1.4$. After including the bright end seen by ASCA for $S > 10^{-13}$ erg s $^{-1}$ cm $^{-2}$ (Della Ceca et al. 2000), the total resolved hard X–ray background amounts to $(1.56 \pm 0.26) \times 10^{-11}$ erg s $^{-1}$ cm $^{-2}$ deg $^{-2}$. In Figure 2 (left) we show the total contribution computed from the CDFS plus ASCA sample. The value at the limiting flux has now reached the value of the unresolved XRB 1.6×10^{-11} erg s $^{-1}$ cm $^{-2}$ deg $^{-2}$ from UHURU and HEAO-1 (Marshall et al. 1980). More recent values of the 2–10 keV integrated flux from the BeppoSAX and ASCA surveys appear higher by 20–40%. Thus a fraction between 0.98 and 0.65 of the total XRB flux value has now been resolved into discrete sources.

The stacked spectrum of the sources of the total sample is well fitted by a power law with a photon index $\Gamma = 1.375 \pm 0.015$ (errors refer to the 90% confidence level) with $\chi^2_\nu = 1.65$ for a column density fixed to the Galactic value $N_H = 8 \times 10^{19}$ cm $^{-2}$. The average spectrum is consistent with the shape of the unresolved hard background $\langle \Gamma \rangle \simeq 1.4$, confirming previous findings. However, we notice that the average spectrum of the sources is harder at low fluxes. To investigate this behaviour, we divided the

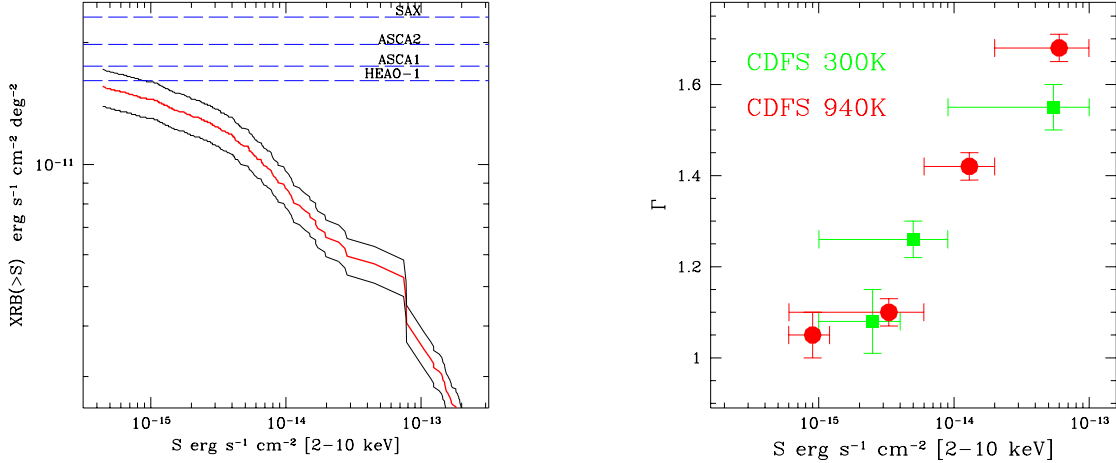


Figure 2: Left: The contribution to the hard X-ray flux density as a function of the flux of the resolved sources (see Rosati et al. 2001). The total resolved contribution is computed from the 1Ms CDFS sample plus the bright sample from ASCA at fluxes larger than $\simeq 10^{-13} \text{ erg s}^{-1} \text{ cm}^{-2}$ (Della Ceca et al. 2000). The upper dashed lines refer to previous measures of the unresolved hard X-ray background; from bottom to top: Marshall et al. (1980, HEAO-1), Ueda et al. (1999, ASCA1), Ishisaki (1999, ASCA2), Vecchi et al. (1999, BeppoSAX). Right: The average power law index of the stacked spectra of the bright, medium, faint and very faint subsamples of the sources detected in the hard band. Errors on Γ refer to the 90% confidence level. The local absorption has been fixed to the Galactic value $N_H = 8 \times 10^{19} \text{ cm}^{-2}$. The squares refer to the 300 ks exposure (Paper II), while the circles to the 1Ms exposure.

sample of sources detected in the hard band in 4 subsamples: bright ($S > 2 \times 10^{-14} \text{ erg s}^{-1} \text{ cm}^{-2}$), medium ($2 \times 10^{-14} > S > 6 \times 10^{-15} \text{ erg s}^{-1} \text{ cm}^{-2}$), faint ($S < 6 \times 10^{-15} \text{ erg s}^{-1} \text{ cm}^{-2}$), and very faint ($S < 2 \times 10^{-15} \text{ erg s}^{-1} \text{ cm}^{-2}$). The average slope of the stacked spectra is $\Gamma = 1.68 \pm 0.03$, 1.42 ± 0.03 , 1.10 ± 0.03 , and 1.05 ± 0.05 respectively (Figure 2, right). These data show the emergence of the hard population at faint fluxes, which resolves the so called *spectral paradox*. In fact, the spectrum of the sources detected from previous X-ray missions (namely ROSAT and ASCA) at fluxes brighter than $10^{-13} \text{ erg s}^{-1} \text{ cm}^{-2}$, showed a spectral slope of $\Gamma \simeq 1.7 - 1.8$. Chandra and XMM have now made possible the direct detection of a population, of absorbed (TypeII) AGNs with hard-band luminosities in the range $L = 10^{42} - 10^{44} \text{ erg s}^{-1}$, building up the flat spectrum ($\Gamma = 1.4$) of the XRB. Softer sources appear to span the range from 10^{40} to $10^{45} \text{ erg s}^{-1}$. At luminosities larger than $10^{43} \text{ erg s}^{-1}$ in the soft band, these sources are mostly identified with TypeI AGN. At the low luminosity end, several sources are detected only in the soft band and are identified with normal galaxies at redshifts less than 0.6, with luminosities restricted to $L_x = 10^{40} - 10^{42} \text{ erg s}^{-1}$ (see also Hornschemeier et al. 2001). Such luminosities may be due to a combination of low-level nuclear activity, a population of low mass X-ray binaries, and thermal emission from hot halos.

3 Comparison with other deep fields

In the CDFS the normalization K (computed at $2 \times 10^{-15} \text{ erg s}^{-1} \text{ cm}^{-2}$) for the hard counts is $\sim 40\%$ lower than that in the Hawaii Deep Field (Mushotzky et al. 2000; see the inset of Figure 1). The difference is statistically significant despite the small area of the Hawaii DF (see Paper I and II). Therefore we investigated if we must revise upwards the fraction of the resolved XRB in the CDFS. To understand the nature of this discrepancy, we analyzed the ACIS-S chip of the Hawaii DF with our procedure. We found the same normalization of the number counts, confirming that the mentioned discrepancy is not due to calibration or detection technique.

To investigate further this issue and estimate the occurrence of this high normalization, we analyzed

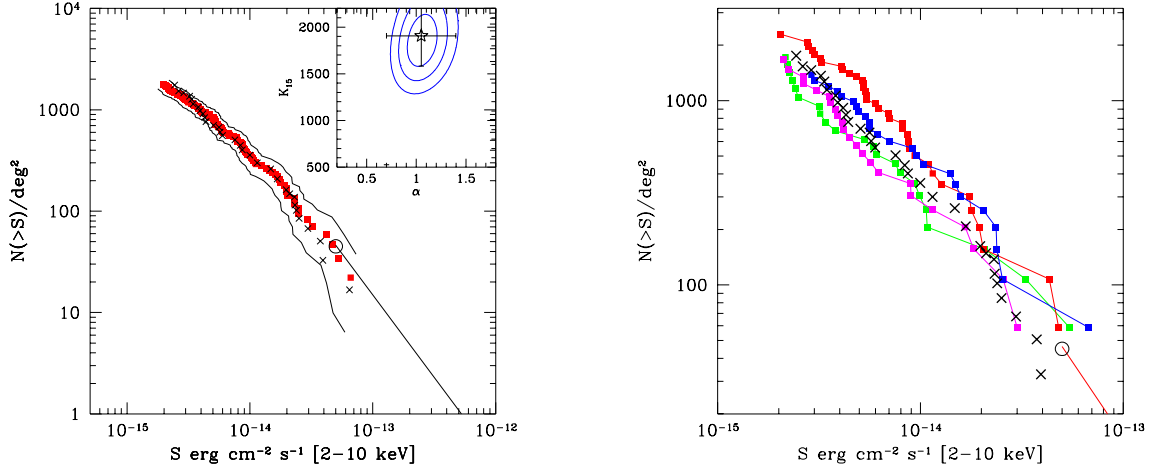


Figure 3: Left: Hard counts from the MS–1137 field (filled squares) compared to the number counts in the Hawaii DF (crosses, Mushotzky et al. 2000) and the corresponding likelihood contours in the inset (see also Figure 1). Right: hard number counts in the MS–1137 field for each of the 4 ACIS–I chips (filled squares) compared to the Hawaii DF counts.

two ACIS–I, public Chandra fields, the Lynx (Stern et al. 2001), and the MS–1137 field. In the first case we found perfect agreement with the CDFS results (see Stern et al. 2001). In the second case, we found the same “excess” of the 0.025 deg² of the Hawaii DF, as shown in Figure 3 (left). However, the excess is given mainly by two chips where the density of sources is significantly larger (Figure 3, right). The remaining properties of this field are perfectly consistent with the CDFS, for example the stacked spectrum of the sources is well fitted by a power law with $\Gamma = 1.39 \pm 0.04$, with the local absorption fixed to the Galactic value of 1.1×10^{20} cm⁻².

Therefore, we find again evidence for positive fluctuations of the hard sources on $\simeq 10$ arcmin scale. This positive fluctuations maybe due to clustering of the hard sources. It is noteworthy to mention that the same effect is not found in the soft band. In fact, we already know that most of the hard sources are in a limited range of redshifts around 1, while the soft sources span a very large range (see Paper II), washing out possible effects of clustering.

How much do these positive fluctuations alter our estimate of the resolved XRB? To summarize our investigation of Chandra deep fields to date, we have 0.33 deg² with a consistent normalization (CDFS, CDFN, Lynx, Lockman Hole), and 0.089 deg² with a $\sim 40\%$ higher normalization (Hawaii DF, MS–1137 field). Considering a 40% higher contribution on 20% of the sky, the resolved contribution in the investigated flux range ($S < 10^{-13}$ er s⁻¹² cm⁻²) rises to $(1.42 \pm 0.22) \times 10^{-11}$ erg s⁻¹ cm⁻² deg⁻². This would bring the total resolved value for $S > 4.5 \times 10^{-16}$ to $(1.67 \pm 0.26) \times 10^{-11}$ erg s⁻¹ cm⁻² deg⁻². This value is $\simeq 7\%$ higher than the CDFS value, but still within the estimated error.

4 Groups and Clusters

Another important population of objects in the CDFS, despite its small solid angle, is constituted by groups and clusters of galaxies. The systematic search for extended source found about 20 detections, including diffuse halos around elliptical galaxies. Here we focus on the three brightest extended sources detected at the level of $S \sim 1 - 3 \times 10^{-15}$ erg s⁻¹ cm⁻² and associated to groups of galaxies. We have redshift for the brightest cluster member of one of them ($z \sim 0.7$), while the optical colors of the others are consistent with being moderate–redshift poor clusters or groups. The stacked spectrum is well fitted by a Raymond–Smith thermal spectrum with temperature $kT = 1.7^{+0.6}_{-0.4}$ keV and a metallicity of $Z = 0.3Z_{\odot}$, after assuming an average redshift of $z \sim 0.5$. The luminosities are in the range $L \simeq 2 - 8 \times 10^{42}$ erg s⁻¹ in the soft band. To this small sample, we can add the three clusters found in the Lynx field at redshifts 0.57 and 1.26 and 1.27 (Holden et al. 2001, Stanford et al. 2001), and

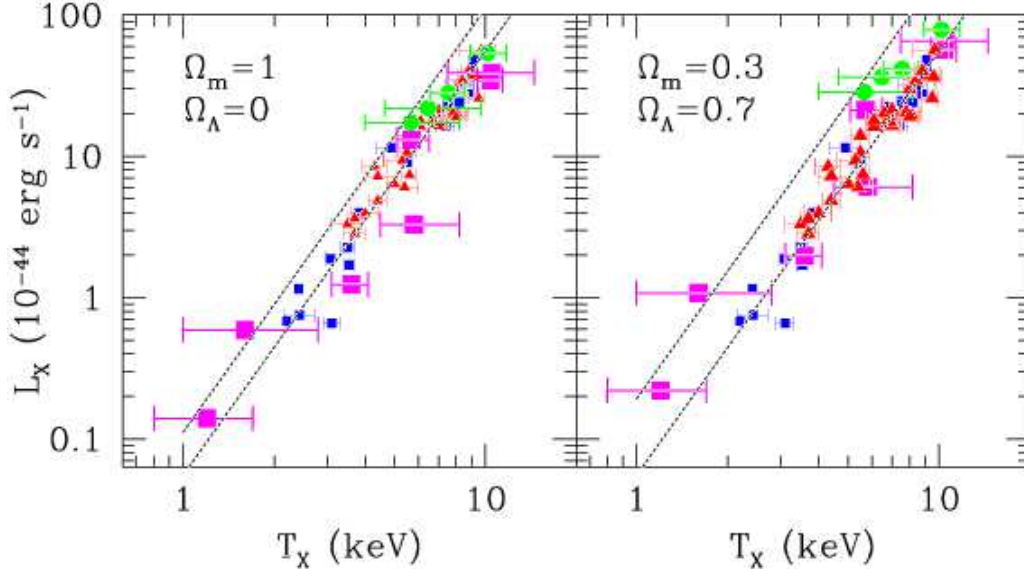


Figure 4: The Luminosity–Temperature relation for nearby and distant clusters in two different cosmologies ($h = 0.5$). The nearby clusters analyzed by Markevitch (1998) and by Arnaud & Evrard (1999) are indicated with small triangles and squares respectively. The large squares are for the compilation of distant ($0.57 \leq z \leq 1.27$) clusters recently observed with Chandra (see Borgani et al. 2001).

the cluster MS–1137 at $z = 0.78$. If we plot these clusters in the L – T plane, together with other two objects from the literature (see Borgani et al. 2001), we find that these sources are consistent with the local L – T relation. This confirms the finding of lack of evolution in the L – T relation (Mushotzky & Scharf 1997) up to $z \sim 1$. This behaviour is expected on the basis of pre–heating models for the ICM (see, e.g., Tozzi & Norman 2001).

5 Conclusions

In these Proceedings we reviewed some of the results from the 1Ms exposure of the CDFS (Rosati et al. 2001). We reached a flux limit of $5.5 \times 10^{-17} \text{ erg s}^{-1} \text{ cm}^{-2}$ in the 0.5–2 keV soft band and $4.5 \times 10^{-16} \text{ erg s}^{-1} \text{ cm}^{-2}$ in the 2–10 keV hard band. For the hard counts, after the inclusion of the ASCA sources at the bright end, the total contribution to the resolved hard X–ray background down to our flux limit now amounts to $(1.56 \pm 0.16) \times 10^{-11} \text{ erg cm}^{-2} \text{ s}^{-1} \text{ deg}^{-2}$. With this new data we resolved 65–98% of the hard XRB, given the uncertainties in the unresolved value, which ranges from 1.6 to $2.4 \times 10^{-11} \text{ erg s}^{-1} \text{ cm}^{-2} \text{ deg}^{-2}$.

The general properties of the X–ray background are now well established. We confirm the finding of a progressive hardening of the sources at lower fluxes, both for the soft and the hard samples. In particular, we divided the hard sample into four subsamples and found average power laws of $\Gamma = 1.68 \pm 0.03$, $\Gamma = 1.42 \pm 0.03$, $\Gamma = 1.10 \pm 0.03$, $\Gamma = 1.05 \pm 0.05$ for the bright, medium, faint and very faint subsample respectively. The progressive hardening at faint fluxes is probably due to a stronger intrinsic absorption. The so called “spectral paradox” is solved by a hard, faint population of sources constituted mostly by nearby ($z \leq 1$) absorbed (Type II) AGN with hard luminosities $L \simeq 10^{42} - 10^{44} \text{ erg s}^{-1}$. Comparison with other deep fields from Chandra, shows that the AGN found in the CDFS are representative of the AGN population as a whole. Some fields have a $\sim 40\%$ higher normalization probably due to clustering of nearby, hard sources. This excess, averaged over the 6 deep fields mentioned and briefly reviewed here, can result in an upward revision of the value of the resolved XRB of about 7%.

We reviewed also the spectral analysis of the three brightest extended sources detected in the CDFS. They are associated with moderate redshift groups of galaxies ($z \simeq 0.5 - 0.7$) and their average

spectrum is well fitted by a Raymond–Smith model with a temperature of $kT = 1.7 \pm 0.4$ keV. This result, added to the three clusters found in the Lynx field, the cluster MS–1137 and other two objects from the literature (see Borgani et al. 2001), shows that there is no hints of evolution of the L – T relation up to $z \simeq 1$. This behaviour is expected in preheating model for the ICM.

The results on AGNs and Clusters reviewed here, give an example of the high–quality performance of the Chandra satellite. In particular, the growing number of deep fields in the Chandra Archive will permit a detailed exploration of the $z \simeq 1$ Universe in X–rays.

References

- [1] Arnaud, M., & Evrard, A.E. 1999, MNRAS, 305, 631
- [2] Borgani, S., Rosati, P., Tozzi, P., et al. 2001, ApJ in press & Squires, G..
- [3] Brandt, W.N., et al. 2000, AJ, 119, 2349
- [4] Della Ceca, R., Braito, V., Cagnoni, I., & Maccacaro, T. 2000, astro-ph/0007430
- [5] Gendreau, K.C., et al. 1995 Publ. Astron. Soc. Jpn. 47, L5-L9
- [6] Giacconi, R., Rosati, P., Tozzi, P., et al. 2001, ApJ, 551, 624 (Paper I)
- [7] Giommi, P., Perri, M., Fiore, F. 2000, A&A, 362, 799
- [8] Hasinger, G., Burg, R., Giacconi, R., Hartner, G., Schmidt, J., Truemper, J., & Zamorani, G. 1993, A&A 275, 1
- [9] Hasinger, G., Burg, R., Giacconi, R., Schmidt, J., Truemper, J., & Zamorani, G. 1998, A&A 329, 482
- [10] Hasinger, G., et al. 2001, A&A 365, L45
- [11] Holden, B. et al. 2001, ApJ in press (astro-ph/0105011)
- [12] Hornschemeier, A.E., et al. 2000, ApJ, 541, 49
- [13] Hornschemeier, A.E., et al. 2001, astro-ph/0101494
- [14] Ishisaki, Y., et al. 1999, ApJ submitted
- [15] Marshall, F. et al. 1980, ApJ, 235, 4
- [16] Markevitch, M. 1998 ApJ, 504, 27
- [17] Mushotzky, R. F., & Scharf, C. A. 1997, ApJ, 482, 13
- [18] Mushotzky, R.F., Cowie, L.L., Barger, A.J., & Arnaud, K.A. 2000, Nature, 404, 459
- [19] Rosati, P., et al. 2001, ApJ submitted (Paper III)
- [20] Stanford A., et al. 2001, ApJ, 552, 504
- [21] Stern, D., et al. 2001, AJ submitted
- [22] Tozzi, P., & Norman, C. 2001, ApJ, 546, 63
- [23] Tozzi, P., et al. 2001, ApJ in press, astro-ph/0103014 (Paper II)
- [24] Ueda, Y., et al. 1999, ApJ, 518, 656
- [25] Vecchi, A., Molendi, S., Guainazzi, M., Fiore, F., & Parmar, A.N. 1999, A&A, 349, 73